




Cite this: *J. Mater. Chem. B*, 2023, 11, 10464

## A photocrosslinked methacrylated carboxymethyl chitosan/oxidized locust bean gum double network hydrogel for cartilage repair†

Can Cheng,<sup>a</sup> Xu Peng,<sup>ab</sup> Yihao Luo,<sup>a</sup> Shubin Shi,<sup>a</sup> Ling Wang,<sup>a</sup> Yuhang Wang<sup>a</sup> and Xixun Yu  <sup>✉</sup>

Repairing articular cartilage defects is a great challenge due to the poor self-regenerative capability of cartilage. Inspired by active substances found in the natural cartilage extracellular matrix, we used methacrylated carboxymethyl chitosan (MA-CMCS) and oxidized locust bean gum (OLBG) as the hydrogel backbone, and prepared a photocrosslinked dual network hydrogel containing allicin and decellularized cartilage powder (DCP). The rheological, swelling and water retention capacities of MA-CMCS@OLBG-Allicin/DCP (MCOAC) hydrogels were investigated to confirm the successful preparation of hydrogels suitable for cartilage repair. The MCOAC hydrogels showed good antibacterial ability to kill *S. aureus* and *E. coli* and anti-inflammatory properties due to the introduction of allicin. Furthermore, MA-CMCS@OLBG-Allicin/DCP hydrogels presented good cytocompatibility due to the addition of DCP, which could promote chondrocyte proliferation and promote the differentiation of BMSCs to chondrocytes. Further studies *in vivo* demonstrated that the DCP-contained MCOAC hydrogel exhibited superior performance in promoting cartilage tissue growth and wound healing in articular cartilage defects. Thus, the MCOAC hydrogel is a promising cartilage repair hydrogel with potential for clinical use.

Received 28th July 2023,  
Accepted 16th October 2023

DOI: 10.1039/d3tb01701j

rsc.li/materials-b

### 1. Introduction

Articular cartilage (AC) is a specialized connective tissue that resists compressive forces and provides a low friction surface for a diarthrodial joint to pivot.<sup>1</sup> Once cartilage defects occur, due to its avascular nature and low cell proliferation/migration, the limited self-repair capability of tissue is insufficient, and no significant regeneration will occur.<sup>2</sup> In the clinic, osteochondral autografts<sup>3</sup> and autologous chondrocyte implantation (ACI)<sup>4</sup> are common strategies for the repair of cartilage defects. However, these two strategies often impair joint function due to the formation of fibrocartilage.<sup>5</sup>

Hydrogels possess cartilage tissue-like characteristics, so their development is now the frontline of research into the treatment of cartilage defects.<sup>6</sup> Hydrogels have a three-dimensional network structure that can absorb large amounts of water while retaining their structure.<sup>7</sup> Hydrogels composed

of synthetic polymers (such as poly(vinyl alcohol) (PVA)<sup>8</sup> and poly(ethylene glycol) (PEG)<sup>9</sup>) are able to exhibit high mechanical strength and good reproducibility but tend to be poorly biocompatible.<sup>10</sup> Therefore, hydrogels prepared from natural macromolecules including polysaccharides, proteins and peptides with excellent biocompatibility are widely used in cartilage repair research.<sup>11</sup> Among the hydrogels, injectable hydrogels have received a lot of attention not only for their unique biological and physicochemical properties (such as cytocompatibility, high water retention and tunable mechanical properties) but also for their ability to fill any shaped wound.<sup>12,13</sup>

Carboxymethyl chitosan (CMCS) is a water-soluble chitosan derivative with good water solubility, gelling properties and biocompatibility.<sup>14</sup> Meanwhile, CMCS possesses several bioactivities, such as antioxidant, antimicrobial and anticancer effects.<sup>15,16</sup> Thus, CMCS has good application potential in food, cosmetic and biomedical industries.<sup>17–19</sup> Research showed that CMCS and strontium ions could form a new polysaccharide complex that could promote the secretion of type II collagen and effectively reduce articular cartilage damage and subchondral bone degradation.<sup>20</sup> Locust bean gum (LBG) is a high molecular weight branched polysaccharide obtained from carob trees.<sup>21</sup> LBG belongs to a family of galactomannan

<sup>a</sup> College of Polymer Science and Engineering, Sichuan University, Chengdu 610065, P. R. China. E-mail: yuxixun@163.com

<sup>b</sup> Experimental and Research Animal Institute, Sichuan University, Chengdu 610065, P. R. China

† Electronic supplementary information (ESI) available. See DOI: <https://doi.org/10.1039/d3tb01701j>

containing a structure of (1-4)- $\beta$ -D-mannopyranosyl backbone with an attachment of (1-6)- $\alpha$ -D-galactose single units.<sup>22</sup> LBG exhibits many salient features, such as high hydrophilicity, excellent biocompatibility, good acid/alkali resistance and high strength.<sup>23,24</sup> Simultaneously, the abundant surface functional groups of LBG make it possible to combine with other materials for synthesizing new materials with excellent performance.<sup>25,26</sup> Matar *et al.* synthesized a LBG/PVA hydrogel using the gel casting method, which exhibited good pH and temperature-responsive behavior and could be used as a candidate biomaterial for drug delivery applications.<sup>27</sup> Kaity *et al.* designed an acrylamide-grafted copolymer of LBG through microwave irradiation and were able to achieve controlled release of bupivacaine hydrochloride.<sup>28</sup>

Meanwhile, decellularized cartilage extracellular matrix (D-cartilage)-derived materials have been used to engineer cartilage grafts with promising results.<sup>29,30</sup> In addition, such D-cartilage-derived biomaterials have been used to bind and release chondrogenic factors, such as transforming growth factor- $\beta$ 3 (TGF- $\beta$ 3).<sup>31</sup> Furthermore, D-cartilage powder (DCP) has also been used to functionalize other biomaterials in an attempt to enhance chondrogenesis.<sup>32,33</sup> Jetze *et al.* designed a gelatin methacrylamide hydrogel with embedded cartilage-derived matrix particles, which could form mineralized bone tissue and showed good cartilage repair ability.<sup>34</sup> Zhang *et al.* promoted type II collagen gene expression and human synovium-derived mesenchymal stem cell proliferation by adding an acellular cartilage matrix to collagen gels.<sup>35</sup>

In this study, we introduced a methacrylate group, a kind of photoreactive group, to synthesize photocrosslinkable methacrylated carboxymethyl chitosan (MA-CMCS). Next, it was used with oxidized locust bean gum (OLBG) to prepare an injectable double network structure hydrogel (MCO). Furthermore, DCP and allicin were added to the hydrogel (MCOAC). The DCP could improve the ability of the hydrogel to promote the cartilage repair. Allicin could cross-link with the hydrogel through its own double bonds, which could improve the stability of the hydrogel and impart antibacterial and anti-inflammatory abilities to the hydrogel.<sup>36,37</sup> The structures of MA-CMCS and OLBG were characterized and the rheological behavior, water absorption and water retention of MCOAC were evaluated. The effects of hydrogels on chondrocytes, mesenchymal stem cells and macrophages as well as antibacterial ability were also estimated through relevant tests. Moreover, the cartilage repair ability of MCOAC *in vivo* was evaluated using a rabbit knee cartilage defect model.

## 2. Materials and methods

### 2.1. Materials

CMCS (MW  $\sim$  100 KDa, deacetylation degree: 90%, substitution degree: 85%) and LBG (MW  $\sim$  310 KDa) were purchased from Beijing Solarbio Technology Co., Ltd. Methacrylic anhydride (MA) was obtained from Sigma-Aldrich (St Louis, USA). Fetal bovine serum (FBS), streptomycin, penicillin, trypsin, Cell

Counting Kit-8 (CCK-8), Dulbecco's Modified Eagle Medium (DMEM), Minimum Essential Medium  $\alpha$  (MEM- $\alpha$ ), and Ham's F12 nutrient medium (F12) were purchased from Gibco BRL (Grand Island, NY, USA). *Escherichia coli* (*E. coli*), *Staphylococcus aureus* (*S. aureus*), chondrocytes, rat bone marrow mesenchymal stem cells (BMSCs) and murine-derived macrophage cell line RAW 264.7 (RAW264.7) were purchased from West China Hospital of Sichuan University. All the reagents and solutions used in this study were of reagent grade.

### 2.2. Preparation of MA-CMCS and OLBG

MA-CMCS was synthesized as reported previously.<sup>38,39</sup> Briefly, 2 g of CMCS was dissolved in 200 ml of deionized water. After heating to dissolve, 4 ml of MA was slowly added at a speed of 0.5 ml min<sup>-1</sup>. The reaction was continued for 4 h at 70 °C. Furthermore, deionized water was used to dialyze MA-CMCS until there were no unreacted small molecules in dialysate (with a molecular weight cutoff of 13 kDa). The solution was collected and lyophilized to obtain the MA-CMCS product.

OLBG was prepared according to our previously reported method.<sup>40</sup> In short, LBG (1 g) was added to 200 ml of deionized water. After complete dissolution, 0.5 g of sodium periodate was added to the solution and then stirred at 600 revolutions per min in the dark at the room temperature for 24 h. Then, 10 ml of ethylene glycol was added and stirred for 2 h to remove unreacted periodate. After completing the reaction, the products were dialyzed against deionized water for 7 d (with a molecular weight cutoff of 3600). The purified OLBG was then lyophilized to obtain the final product.

The chemical structure of CMCS, MA-CMCS, LBG and OLBG was characterized by Fourier transform infrared (FTIR) and <sup>1</sup>H nuclear magnetic resonance (<sup>1</sup>H NMR) spectroscopy. The details of the methods are available in the ESI.†

### 2.3. Decellularization of cartilage

The fresh porcine rib cartilage, which was obtained from Animal Experiment Center of Sichuan University, was stored at -80 °C. Phosphate-buffered saline (PBS) solution was used to rinse off the excess tissue and fascia on the surface of cartilage before use. Then, the cartilage was sliced into thin slices (about 3 mm) using a scalpel. The prepared cartilage was immersed in a 4% SDS/PBS solution at 37 °C for 24 h, and the residual SDS was washed away using PBS solution. Then, 1% Triton X-100/PBS solution was used to further decellularize cartilage for 24 h, after that, PBS solution was used repeatedly to remove the residual decellularization fluid and cell debris. Then, the obtained decellularized cartilage (D-cartilage) was frozen at -80 °C for further use. The sample was embedded in the optimal cutting temperature compound (O. C. T) at -20 °C and then sectioned into 7  $\mu$ m thick slices for hematoxylin and eosin (H&E) staining. A light microscope was employed to observe specimens. Moreover, the DNA and collagen II (Col-2) in fresh and decellularized cartilage were determined using spectrophotometry with appropriate assay kits. Finally, the specimens subjected to critical point-drying and sputter gold

coating were examined using scanning electron microscopy (SEM) to observe the microstructure of the cartilage.

The lyophilized decellularized cartilage was ground into particles, and then it was further ground using a cryoball mill to obtain decellularized cartilage powder (DCP).<sup>41</sup> In brief, cartilage was precooled for 3 min prior to pulverization at 5 Hz for 10 cycles of 1 min cooling. The particle size of DCP was observed *via* SEM and the elemental distribution of DCP was observed through EDS mapping. The powder was stored in a  $-80^{\circ}\text{C}$  environment for subsequent backup.

#### 2.4. Preparation of MA-CMCS@OLBG-AC hydrogels

2.5 g of MA-CMCS was dissolved in 20 ml of deionized water and completely dissolved at  $70^{\circ}\text{C}$ . Then 0.5 g of OLBG was added to the system, resulting in a homogeneous MA-CMCS/OLBG mixture obtained after complete dissolution of OLBG. 50 mg of Irgacure 2959 was added to the mixture and after being dissolved completely, 100  $\mu\text{l}$  allicin was added to the system (MA-CMCS@OLBG-A). After the reaction system was cooled to room temperature, the specified concentration of cartilage powder (0 mg, 50 mg, 100 mg, 150 mg, 200 mg, and 250 mg) was added. Finally, after ultrasonic dissolution, the hydrogel was obtained using UV light (365 nm, 20  $\text{mW cm}^{-2}$ , 60 s) to initiate polymerization.

The hydrogels with different concentrations of cartilage were named as: MCOA, MCOAC-50, MCOAC-100, MCOAC-150, MCOAC-200 and MCOAC-250.

#### 2.5. Physicochemical characterization of hydrogels

**2.5.1. Morphology of hydrogels.** The morphology of hydrogels was observed *via* SEM. Briefly, the hydrogel precursor solution was added to a 24-well plate, and after UV-initiated polymerization, the hydrogels were frozen at  $-80^{\circ}\text{C}$ . After lyophilizing and spraying gold, the hydrogels' morphology was observed *via* SEM.

**2.5.2. Rheological properties.** Rheological measurements of MCOAC hydrogels were performed using an Anton paar MCR 302 rheometer. A series of MCOAC hydrogels with different concentrations of cartilage were prepared as cylindrical discs with a thickness of 2 mm and a diameter of 15 mm. The sweep time range was from 0 s to 180 s, and the amplitude  $\gamma$  was 0.5%. The strain sweep range  $\gamma$  was from 0.1% to 100%, and the angular frequency was fixed at 1 Hz. During the test, the temperature of the sample stage was kept constant at  $37^{\circ}\text{C}$ .

**2.5.3. Swelling behavior and water evaporation ratio.** The swelling behavior and water evaporation ratio of MCOAC hydrogels were evaluated according to previous publications.<sup>42</sup> The details of the methods are given in the ESI.†

#### 2.6. Antibacterial activity

The plate count method was employed to evaluate the antibacterial behavior of the MCOAC hydrogels and *Staphylococcus aureus* and *Escherichia coli* were used as model bacteria. The details of the methods are given in the ESI.†

#### 2.7. Chondrocyte compatibility

**2.7.1. Cytotoxicity assay.** The cytocompatibility of MCOAC hydrogels was evaluated using chondrocytes *via* the direct contact method. Cells seeded on a 24-well plate without hydrogel served as the control group. And fluorescein diacetyl (FDA) staining was used to study the cell viability of chondrocytes on MCOAC hydrogels. The details of the methods are given in the ESI.†

**2.7.2. Chondrocyte morphology observation.** After incubating the chondrocyte seeded on sterilized hydrogel specimens for four days, their spreading morphology was observed *via* SEM and confocal laser scanning microscopy (CLSM). The details of the methods are given in the ESI.†

**2.7.3. Cytokine determination.** The level of type II collagen (Col-2) and glycosaminoglycan (GAG) protein in supernatant medium were evaluated through ELISA. Various cell-attached hydrogel samples were prepared as detailed above. After incubating for 4 days in a 24-well plate, supernatant liquid was collected for ELISA assays through centrifugation. A standard curve was plotted according to the measurement value of a series concentration of Col-2 and GAG standard solution. Then, the ELISA assay was run according to the manufacturer's instructions (R&D Crop.) to determine the accurate concentration of Col-2 and GAG, and their values were expressed as  $\text{pg ml}^{-1}$ .

#### 2.8. The effect of MCOAC hydrogels on RAW264.7

**2.8.1. Activation of RAW264.7.** The complete medium for RAW264.7 cells consisted of DMEM and 10% FBS. Penicillin-streptomycin was not added to prevent RAW264.7 cells from being activated, and LPS ( $25 \text{ ng ml}^{-1}$ ) was added as an inflammatory stimulator to activate RAW264.7.

**2.8.2. Morphology of RAW264.7.** Inactivated and activated macrophages were cultured in the same way as described above and were seeded at a density of  $5 \times 10^4 \text{ cells ml}^{-1}$  on the surface of hydrogel samples. The cell morphology was observed by CLSM. The details of the methods are given in the ESI.†

**2.8.3. Secretion of inflammatory factors.** To further evaluate the effect of hydrogels on the secretion of inflammatory factors from RAW264.7, we cocultured different hydrogels with RAW264.7 for 4 days and then used ELISA kits to detect TNF- $\alpha$ , IL-1 $\beta$  and IL-6 secreted by RAW264.7.

#### 2.9. The effects of MCOAC hydrogels on BMSCs

**2.9.1. Cytotoxicity assay.** The cytocompatibility of MCOAC hydrogels in BMSCs was evaluated using the same method as mentioned in Section 2.7.1. The details of the methods are given in the ESI.†

**2.9.2. Morphology of BMSCs.** BMSCs were cultured in the same way as described above and were seeded at a density of  $5 \times 10^4 \text{ cells ml}^{-1}$  on the surface of hydrogel samples. The cell morphology was observed by CLSM. The details of the methods are given in the ESI.†

**2.9.3. Scratch and Transwell assay.** The effect of hydrogels on cell motility was observed through cell scratch and

Transwell experiments.<sup>43</sup> In the scratching experiment, BMSCs were seeded in a 6-well plate and scratched in the culture plate with a pipette tip after 24 h and then cultured with different hydrogels until the specified times (0 h, 12 h, and 24 h). The cell movement was observed under a microscope. Transwell experiment was performed in 24-well Transwell plates. BMSCs were first seeded in the upper chamber and cultured with a serum-free medium. Then a complete medium containing different hydrogels was added to the lower chamber, and the Transwell plate was placed in a 37 °C incubator with 5% CO<sub>2</sub> and incubated for 24 h. The lower chamber was stained with crystal violet dye and observed using a microscope.

**2.9.4. Cytokine determination.** To further assess the ability of MCOAC hydrogels to promote the chondrogenic differentiation of BMSCs. After co-culturing BMSCs with different hydrogels for 7 and 14 days, the expression of Col-2 and GAG proteins was determined using the same method as described in 2.7.3.

## 2.10. *In vivo* cartilage repair

**2.10.1. Animal experiments.** Rabbits (2.5–3.0 kg, female) were purchased from Chengdu Dashuo Animal Co. Ltd and were taken care of according to the guidelines for Care and Use of Laboratory Animals of Sichuan University. Animal experiments were approved by the Animal Ethics Committee of Sichuan University (No. SYDW2021051604) which followed the National Research Council's Guide for the Care and Use of Laboratory Animals. And animal experiments were carried out after confirming the health of rabbits. Briefly, the rabbits were first anesthetized with isoflurane using a respiratory anesthesia machine, and a medial parapatellar approach was used to expose the stifle joint of rabbits and the patella was laterally dislocated. One critical-sized (2.8 mm diameter) full-thickness cartilage defect was created using a surgical puncher with null or minimal damage to the subchondral bone on each femoroacetabular groove. The hydrogel precursor solution was then injected and irradiated by 305 nm UV light for 1 min to initiate polymerization and form a hydrogel *in situ* at the cartilage defect. After 4 and 12 weeks of uneventful healing, the rabbits were euthanized. The femur distal ends including the whole osteochondral parts were collected with complete integrity and the specimens were stored in 4% paraformaldehyde before bone histomorphometric analysis. The defect group without hydrogel was used as the blank control group.

**2.10.2. Patellar wear and knee joint inflammation.** To further evaluate the healing of the cartilage defect, patellae from the knee joint were collected to assess tissue healing during cartilage repair by observing the degree of patellar surface wear. Meanwhile, the fluid in the joint cavity was flushed by saline and then collected, and the TNF- $\alpha$  and IL-1 $\beta$  content in the fluid was measured using an ELISA kit. The details of the methods are given in the ESI.†

**2.10.3. Synchrotron radiation tomography.** To understand the cartilage regeneration at the defect site after 4 weeks and 12 weeks of implant, the formalin-fixed tissues were studied through microtomographic (micro-CT, scanco vivaCT80) observations. The details of the methods are given in the ESI.†

**2.10.4. Histology and immunohistochemistry.** All specimens were paraffin-embedded and then sectioned with a thickness of 10  $\mu$ m through the center of the sample with a microtome. H&E staining and Masson staining were respectively conducted according to the standard protocols.

## 2.11. Statistical analysis

Experimental data were expressed as mean  $\pm$  standard deviation and analyzed using one-way ANOVA on SPSS (version 20.0). *p* value lower than 0.05 was considered statistically significant, *i.e.* \* represents *p* < 0.05, \*\* represents *p* < 0.01.

# 3. Results and discussions

## 3.1. Preparation and characterization of MA-CMCS and OLBG

Photocrosslinking requires functional groups for light curing. For this purpose, CMCS was methacrylated, and the methacrylation process was carried out in the aqueous phase, with methacrylic anhydride (MA) as the methacrylation agent. Under these conditions, the alcohol groups of CMCS reacted with MA, which led to the grafting of methacrylate functional groups along the CMCS backbone (MA-CMCS) (Fig. 1A). Successful methacrylation of CMCS was confirmed *via* FTIR and <sup>1</sup>H NMR spectroscopies.<sup>44,45</sup> FTIR and <sup>1</sup>H NMR spectra of neat CMCS were also recorded for comparison.

The asymmetric (1590 cm<sup>-1</sup>) and symmetric (1413 cm<sup>-1</sup>) stretching vibrations associated with carboxylate (–COO–) were detected in both CMCS and MA-CMCS FTIR spectra, respectively. A broad peak between 3000 and 3700 cm<sup>-1</sup> due to the –OH stretching vibration was also detected. The methacrylated product, MA-CMCS, also showed the characteristic FTIR vibration bonds derived from the –(C=O) O ester group, and the –C–H at 1715 and 811 cm<sup>-1</sup>, respectively (Fig. 1C). The methacrylation of CMCS was further evaluated using <sup>1</sup>H NMR spectra. The spectrum of MA-CMCS showed peaks corresponding to vinyl ( $\delta$  = 5.7 ppm) and methyl ( $\delta$  = 1.9 ppm) groups, which confirmed the presence of methacrylate groups (Fig. 1D).

Sodium periodate can oxidize the *o*-hydroxyl groups in LBG to form dialdehyde groups (Fig. 1B). Furthermore, these aldehyde groups can react with the amino groups in MA-CMCS through the Schiff reaction to achieve crosslinking. The formation of dialdehyde groups in OLBG has been verified *via* FTIR spectroscopy. As shown in Fig. 1E, compared to LBG, a new characteristic peak of aldehydes at 1735 cm<sup>-1</sup> was observed in the spectrum of OLBG. However, this new peak was relatively weak due to the existence of some aldehydes in the form of hemiacetals.

## 3.2. Decellularization results

To systematically evaluate the effect of decellularization, H&E staining was performed on fresh and decellularized cartilage, and the surface morphology of cartilage before and after decellularization was observed *via* SEM, and the content of DNA and Col-2 was quantitatively determined. As shown in Fig. 2A, the nuclei were no longer present in D-cartilage

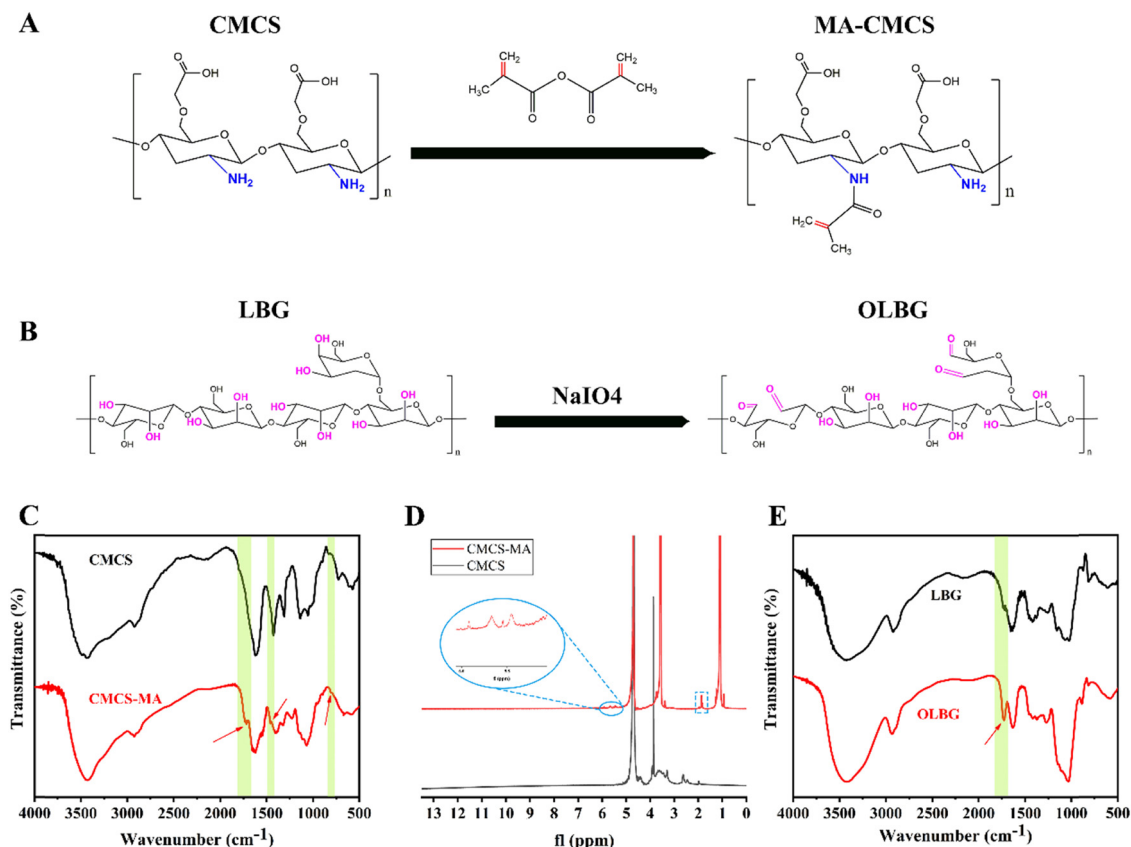


Fig. 1 Structural characterization of MA-CMCS and OLBG. (A) Reaction schematic of MA-CMCS. (B) Reaction schematic of OLBG. (C) FTIR spectra of CMCS and MA-CMCS. (D)  $^1\text{H}$  NMR spectra of CMCS and MA-CMCS and (E) FTIR spectra of LBG and OLBG.

samples, while they were present in large quantities in fresh cartilage specimens. As seen in SEM images (Fig. 2B), spherical chondrocytes distributed in the cartilage capsule could be observed on the surface of fresh cartilage, but only cavities of the cartilage capsule were observed on the surface of D-cartilage. The microscopic morphology of the cartilage surface before and after decellularization was not disrupted. This was also confirmed by the H&E staining images. The DNA content in D-cartilage samples (Fig. 2C) was significantly reduced to  $31.25 \text{ ng mg}^{-1}$ , which was much lower than that of fresh cartilage ( $289.64 \text{ ng mg}^{-1}$ ), meeting the minimum standard for decellularized native tissues ( $< 50 \text{ ng mg}^{-1}$ ).<sup>46</sup> However, we found that the Col-2 content in decellularized specimens (Fig. 2D) was only slightly lower than that in fresh samples, indicating that our decellularization protocol only destroyed the cellular structures in tissue and did not cause damage to the extracellular matrix. Thus, the decellularization method we used can effectively remove cellular components and reduce immune antigenicity.

The low-temperature ball milling can protect the bioactive material in the decellularized cartilage as much as possible. It can be seen from Fig. 2E that the particle size of DCP is roughly  $2\text{--}5 \mu\text{m}$ , which enables the powder to be uniformly dispersed in hydrogels. Meanwhile, the particle size distribution (Fig. S1, ESI<sup>†</sup>) and the monodisperse morphology (Fig. S2, ESI<sup>†</sup>) of DCP were tested to further quantify its diameter. The elemental

distribution map (Fig. 2F) of DCP further indicated that the powder retained the elements of sulfur, oxygen and calcium in the cartilage. However, there was some error in the distribution of carbon elements due to the interference of conductive gel.

### 3.3. Synthesis of MCOAC hydrogels

Our hydrogels fabricated from MA-CMCS, OLBG, allicin and DCP were referred to as MCOAC hydrogels. As shown in Fig. 3A, MA-CMCS and OLBG are used as substrate materials for hydrogels. They both have good biocompatibility, while MA-CMCS can form a cross-linked network after photoinitiation, and the aldehyde group in OLBG is able to form a second layer of the network with the amino group in MA-CMCS *via* the Schiff base reaction, which can improve the structural stability of hydrogels. Allicin was chosen due to its antibacterial and anti-inflammatory properties, and DCP conferred better chondrocyte compatibility to hydrogels as well as the ability to promote differentiation of mesenchymal stem cells to chondrocytes, which are desirable characteristics for cartilage repair hydrogels.

### 3.4. Morphology of the MCOAC hydrogels

Fig. 3B shows the SEM images of lyophilized MCOAC hydrogels. It could be seen from the SEM image that there were a large number of micropores inside the hydrogel and a stable mesh structure was formed. Also, it could be observed that DCP was

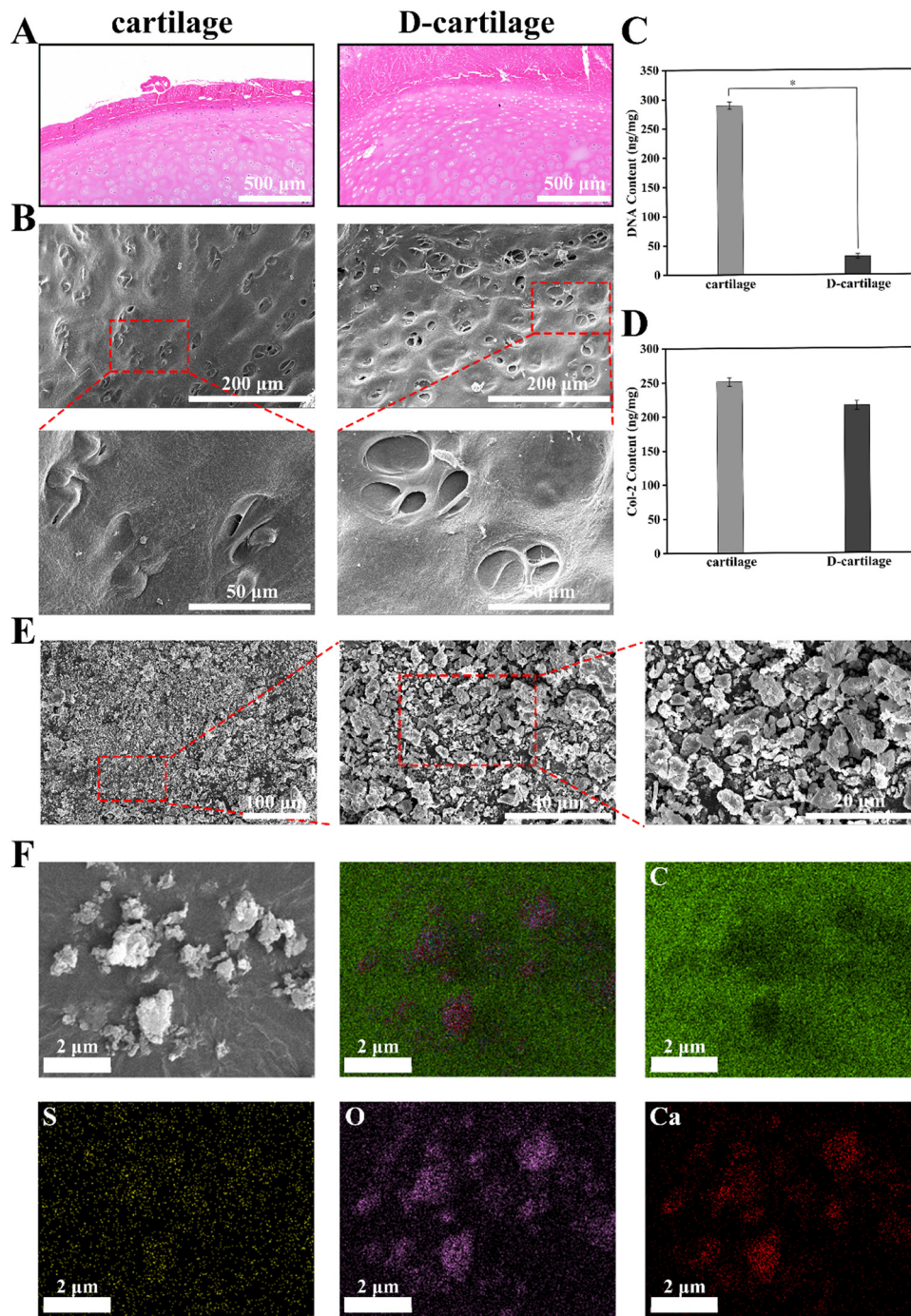


Fig. 2 Characterization of cartilage-decellularization. (A) Standard H&E stain for cartilage and D-cartilage. (B) SEM images for cartilage and D-cartilage. (C) DNA content. (D) Col-2 content. (E) SEM images for DCP. (F) Elemental distribution of DCP. Data are presented as mean  $\pm$  SD ( $n = 6$ ). \* Represents  $p < 0.05$  (two-tailed Student's  $t$ -test).

uniformly dispersed in hydrogel. This further illustrated the stability of a double network structure, and this interlaced pore structure provided microenvironments for stem cell migration and chondrogenic differentiation.

### 3.5. Rheological properties of MCOAC hydrogels

The time sweep rheology of MCOAC hydrogels is shown in Fig. 4A. The storage modulus ( $G'$ ) of all specimens was

one order of magnitude higher than the loss modulus ( $G''$ ), which suggested the formation of hydrogels. Moreover, we found that the more the DCP content in the hydrogel, the greater the values of  $G'$  and  $G''$  in the hydrogel presented. This was because the DCP formed an island-like structure in hydrogel similar to that of the styrene-butadiene-styrene (SBS) elastomer, which could effectively increase the strength of the hydrogel.

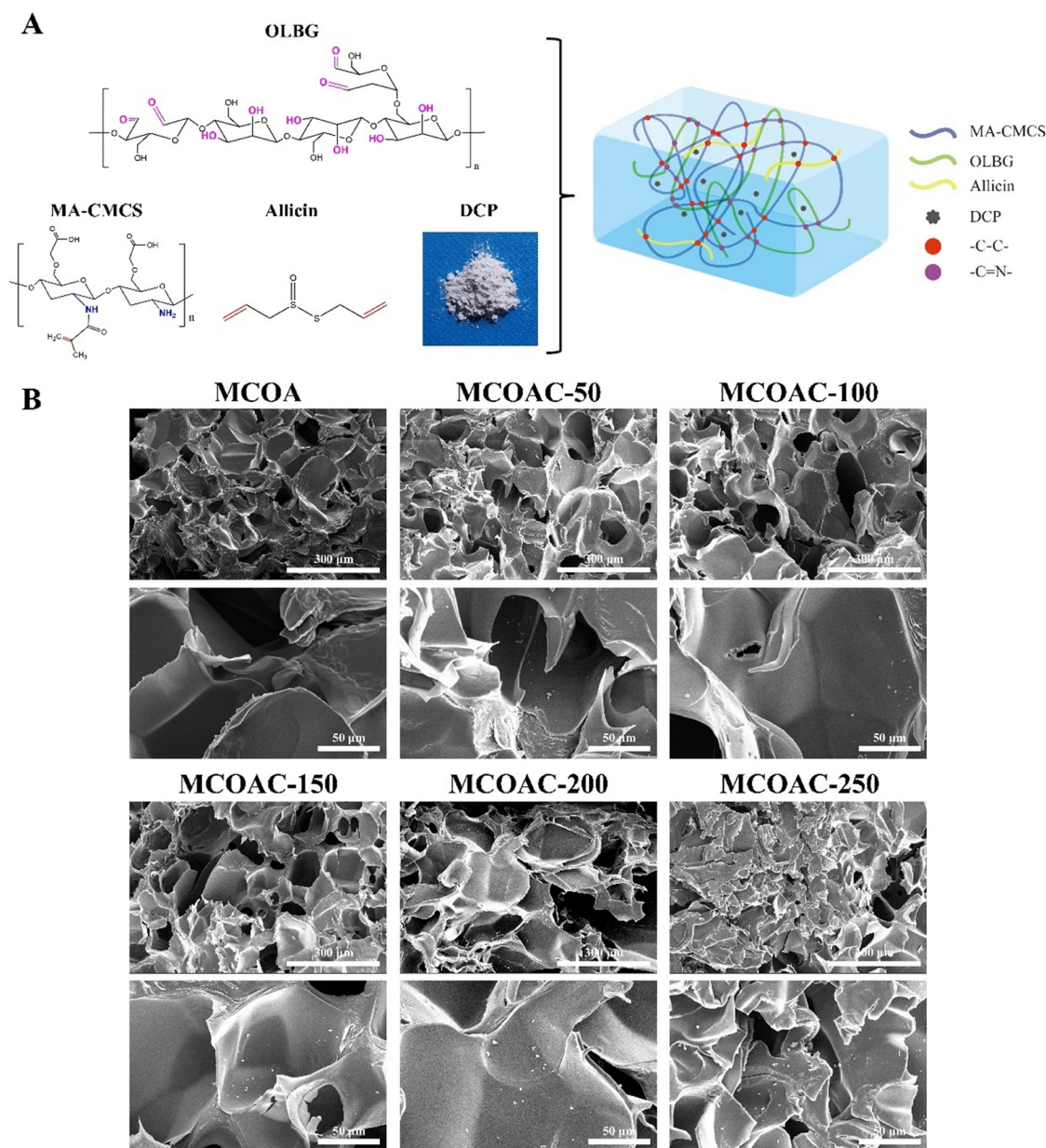


Fig. 3 (A) Diagram for the preparation of hydrogel. (B) SEM images for different MCOAC hydrogels.

The strain sweeps at a fixed angular frequency of 1 Hz (Fig. 4B) showed the dependence of the storage modulus  $G'$  and the loss modulus  $G''$  of MCOAC hydrogels on the strain. When the loss modulus  $G''$  was higher than the storage modulus  $G'$ , the hydrogel collapsed. As the composition of the DCP-forming gel increased, the island-like structure inside the hydrogel increased and the strain resistance of the hydrogel also increased.

### 3.6. Swelling properties and water evaporation ratio

The dynamic swelling behavior of MCOAC hydrogels is shown in Fig. 4C. The swelling process underwent two stages with different swelling speeds. After being immersed in water for about 6 h, all hydrogels almost reached the swelling

equilibrium state, and the swelling speed of hydrogels became slow after 6 h. As the content of DCP increased, the ability of water uptake of the hydrogel decreased. This was because, as a solid component in the hydrogel, DCP did not have a strong water absorption capacity itself, leading to a decrease in the swelling properties of the hydrogel.

The water evaporation ratio of hydrogels with different DCP contents is shown in Fig. 4D. The water evaporation rate of all specimens was fast in the first 24 h and then subsequently slowed down. The MCOAC-250 and MCOAC-200 hydrogels still lost water rapidly after 24 h due to the low water retention capacity of higher content of DCP in the hydrogel. However, MCOAC-150, MCOAC-100 and MCOAC-50 still had good water retention capacity, which facilitated the provision of a moist

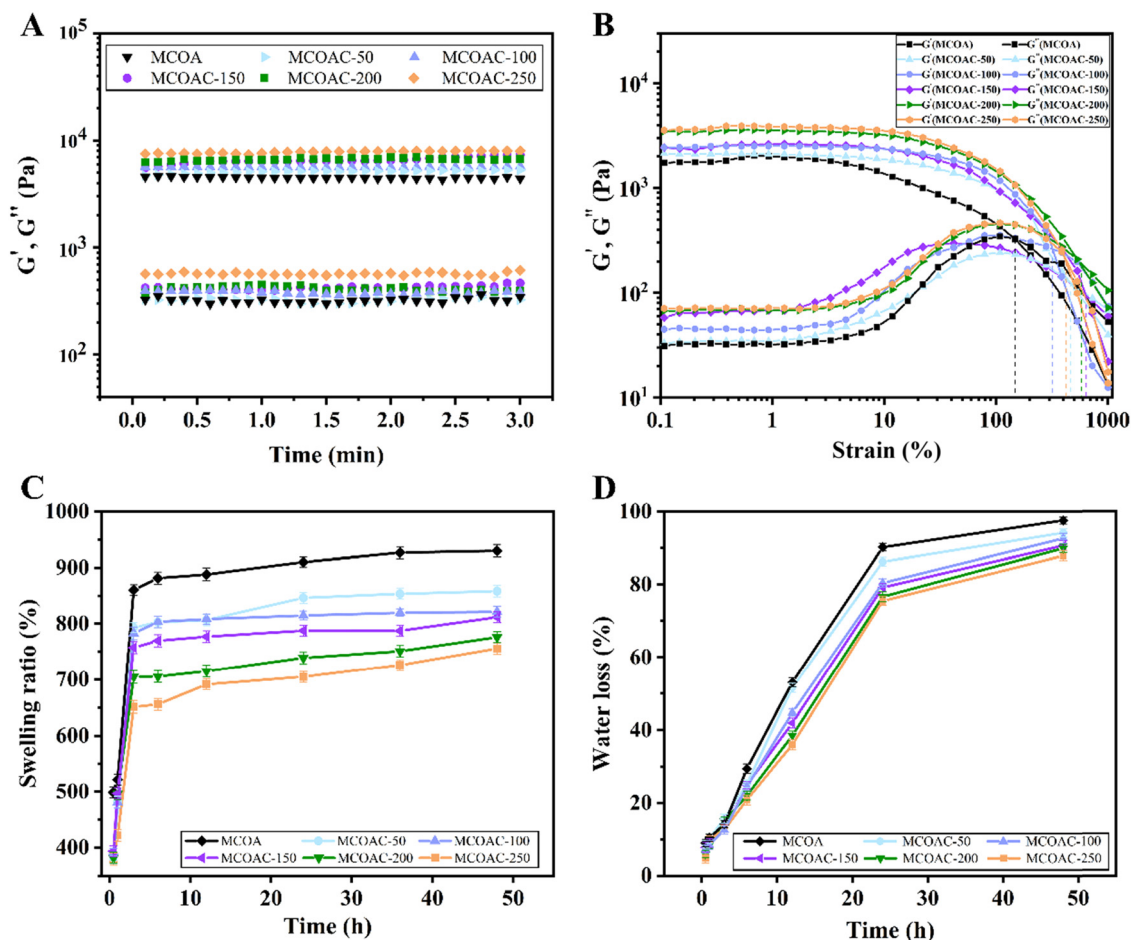


Fig. 4 Characteristics of hydrogels. (A) The time sweep test for different hydrogels. (B) Strain amplitude sweep test for different hydrogels. (C) Swelling ratio of different hydrogels. (D) Water evaporation ratio of different hydrogels.

environment at the cartilage defect site and could alleviate the frictional damage caused by the cartilage defect and improve joint motion.<sup>47</sup>

### 3.7. Antibacterial properties

The antibacterial activity of allicin was closely related to its special chemical structure.<sup>48</sup> Allicin contains thioether groups and allyl groups that inhibit bacterial growth and proliferation by inhibiting the activity of bacterial metabolic enzymes, damaging the cell membrane system of bacteria and affecting the growth environment of bacteria.<sup>49</sup>

As seen in Fig. 5, all hydrogel specimens exhibited good antibacterial ability against *S. aureus* and *E. coli*, which indirectly proved the successful introduction of allicin. However, the antibacterial ability of hydrogels decreased slightly with the increase of DCP content in hydrogel. The antibacterial ratios of different hydrogels against *S. aureus* and *E. coli* were respectively 96.77% and 99.72% for MCOA hydrogel, 93.12% and 99.71% for MCOAC-50 hydrogel, 91.69% and 99.59% for MCOAC-100 hydrogel, 91.58% and 99.52% for MCOAC-150 hydrogel, 90.76% and 98.22% for MCOAC-200 hydrogel, and 83.44% and 96.66% for MCOAC-250 hydrogel. There was no

significant difference among the antibacterial ratios of all hydrogels against *E. coli*. For *S. aureus*, there was no significant difference in the antibacterial ratios between MCOA and MCOAC-50 ~ MCOAC-200, but the antibacterial ratio of MCOAC-250 hydrogel against *S. aureus* decreased to 83.44%, which was much lower than that of MCOA hydrogel. This might be attributed to the increase in DCP content leading to a decrease in the effective concentration of allicin (Fig. S9, ESI†), as well as the ability of bacteria to utilize DCP as a source of nutrients, which ultimately led to a decrease in the antibacterial capacity. In conclusion, MCOAC hydrogels showed good antibacterial ability against *S. aureus* and *E. coli* (antibacterial ratio of all specimens exceeded 90%, except for MCOAC-250), which can effectively reduce the bacterial infections during cartilage repair.

### 3.8. Chondrocyte compatibility

**3.8.1. Cytotoxicity assay.** Cytotoxicity tests were carried out to further evaluate the application of MCOAC hydrogels in the field of biomaterials. As shown in Fig. 6A, the cell viability of chondrocytes was validated using FDA staining of chondrocytes via fluorescence microscopy. The number of chondrocytes on

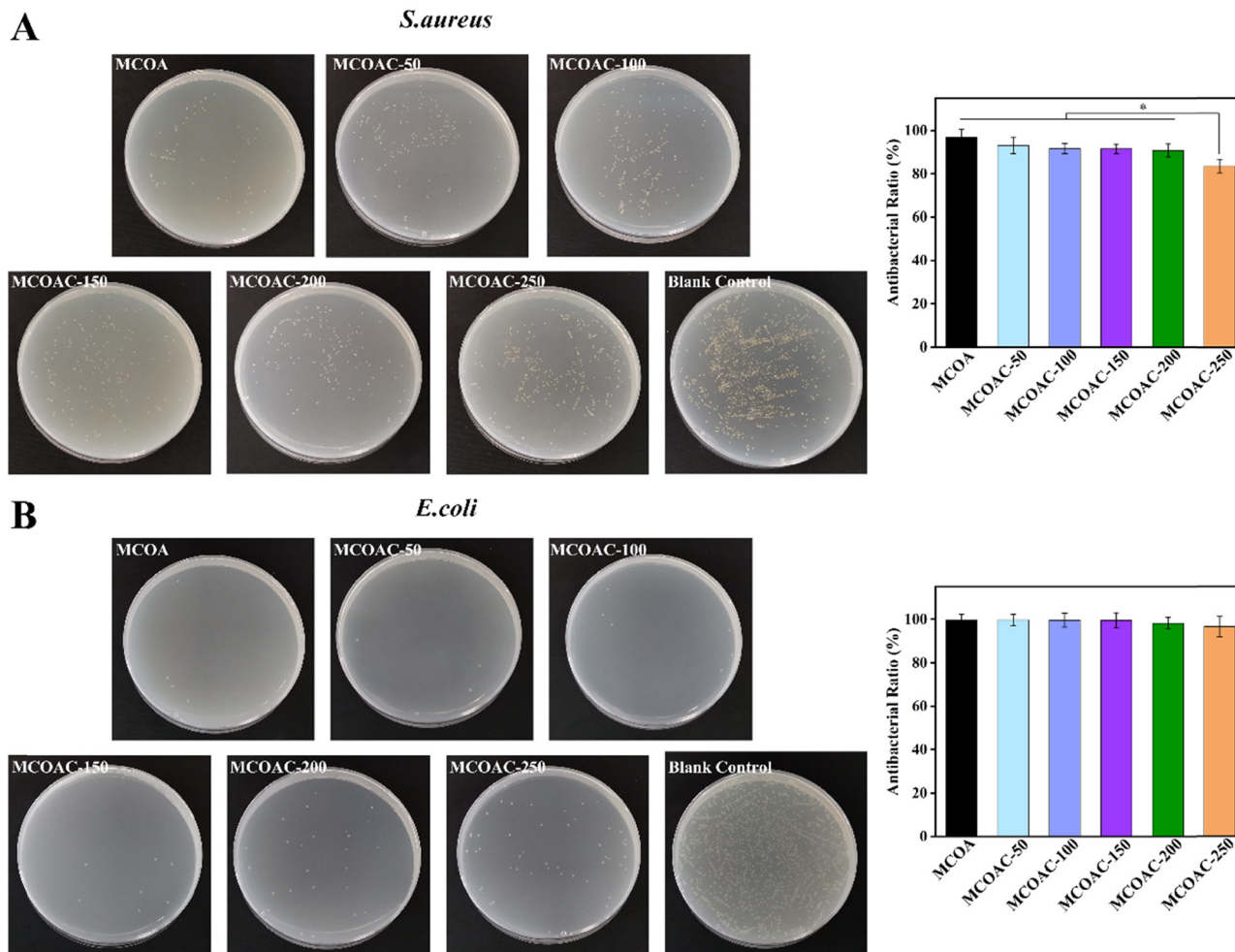


Fig. 5 The antibacterial test on a flat plate. (A) The bactericidal effect of MCOA hydrogels with different concentrations of DCP against *S. aureus*. (B) The bactericidal effect of MCOA hydrogels with different concentrations of DCP against *E. coli*. Data are presented as mean  $\pm$  SD ( $n = 6$ ). \* Represents  $p < 0.05$  (one-way ANOVA).

the surface of MCOA hydrogel was significantly less than the number of chondrocytes on various MCOAC hydrogels, and the largest number of chondrocytes was exhibited on the surface of MCOAC-150 hydrogel. The RGR results further illustrated the cytotoxicity of hydrogel specimens. As shown in Fig. 6B, the chondrocyte-RGRs of all specimens were higher than 75%. And compared with MCOA hydrogel, the DCP-contained MCOAC hydrogels exhibited better chondrocyte-compatibility. With the increase of DCP in hydrogel, the RGR of samples first increased and then decreased, and reached a maximum in the MCOAC-150 hydrogel group. This may be because, with the increase of DCP content, a good microenvironment was provided for chondrocytes, leading to improved chondrocyte-compatibility of hydrogels, but the hydrogels containing excessive DCP content would release a large amount of degraded small molecules during the cell culture process, which was not conducive to cell growth.

**3.8.2. Chondrocyte morphology.** To further validate the results of FDA staining and CCK-8 analysis, the morphology and distribution of chondrocytes on specimens were observed

via SEM and CLSM. As shown in Fig. 6E, only a few cells with poor spreading were observed on the surface of MCOA hydrogel, which represented its low chondrocyte-compatibility. In contrast, a large number of spreading-chondrocytes were observed on the surface of DCP-contained hydrogels, indicating their lower cytotoxicity and good proliferation activity. We also observed the chondrocytes on various DCP-contained hydrogels by CLSM. As shown in Fig. S10 (ESI<sup>†</sup>), the actin microfilaments within chondrocytes on various MCOAC hydrogels were displayed, elongated and oriented, which further demonstrated their good chondrocyte-compatibility.

**3.8.3. Cytokine determination.** Col-2 is the most abundant protein in the cartilage. It is a fibrillar collagen that acts as the structural framework of the cartilage extracellular matrix (ECM).<sup>50</sup> GAG is the main ECM glycoprotein of the articular cartilage, and it is a protein that has been modified by large polyanionic carbohydrates (mainly chondroitin sulfate).<sup>51</sup> It binds to hyaluronic acid and draws cations along with osmotically obligated water into the ECM, forming a hydrated gel which gives cartilage its compressive strength.<sup>52</sup>

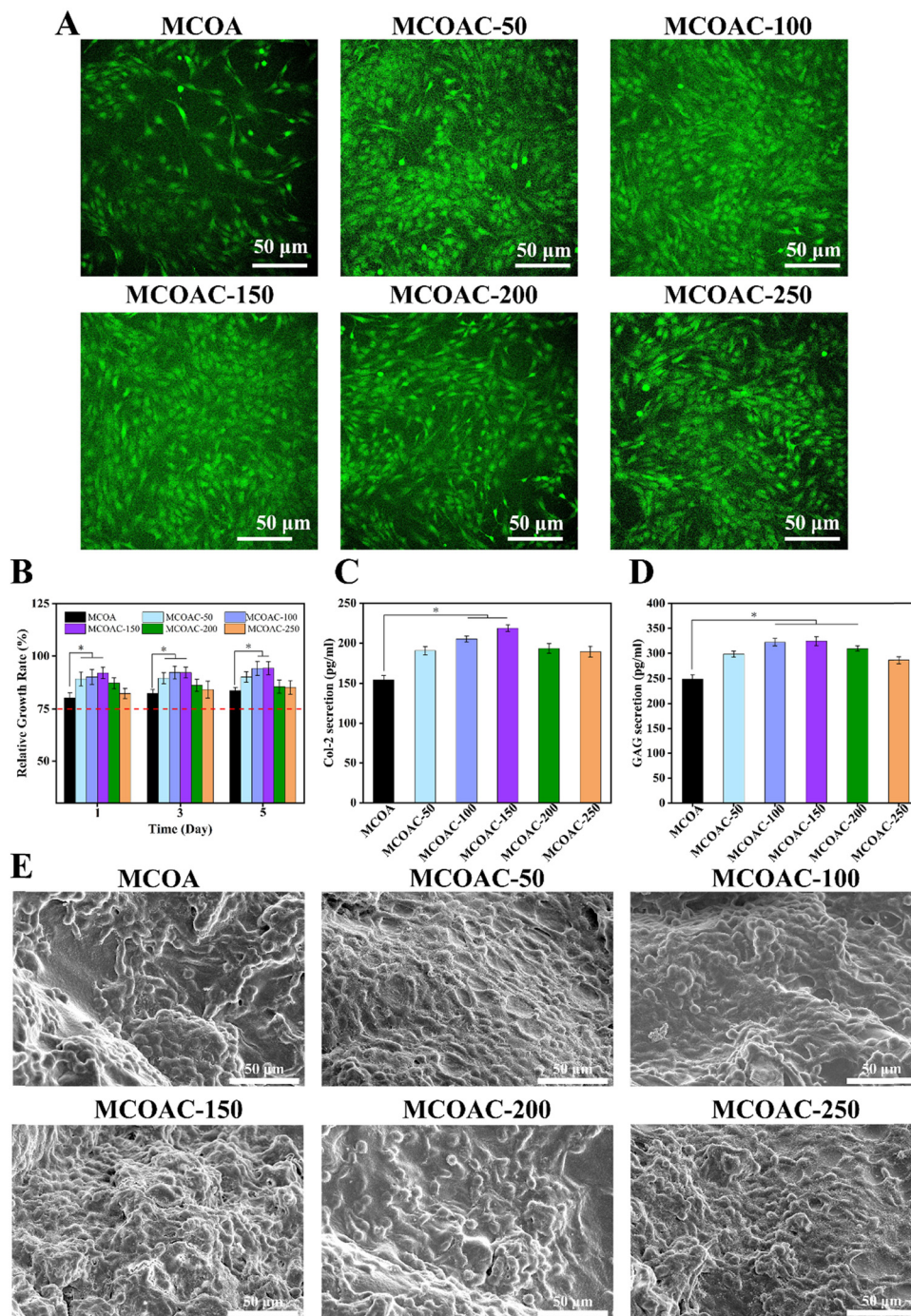


**Fig. 6** The chondrocyte compatibility of hydrogels. (A) The images of living chondrocyte staining by FDA. (B) Cell viability of chondrocyte co-cultured with different hydrogels. (C) Col-2 secretion of chondrocyte. (D) GAG secretion of chondrocyte. (E) SEM images of chondrocyte co-cultured with different hydrogels. Data are presented as mean  $\pm$  SD ( $n = 6$ ). \* represents  $p < 0.05$  (one-way ANOVA).

By determining the expression of Col-2 and GAG from chondrocytes co-cultured with the specimens, we are able to further investigate whether the MCOAC hydrogels have better chondrocyte-compatibility. As shown in Fig. 6C and D, the secretion of Col-2 and GAG from chondrocytes co-cultured with the DCP-contained MCOAC hydrogels was higher than that in the blank hydrogel group, which indicated that DCP could

effectively promote the secretion of Col-2 and GAG by chondrocytes. Meanwhile, the secretion of Col-2 and GAG from chondrocytes in MCOAC-100 and MCOAC-150 groups was highest for all specimens, which was basically consistent with the CCK-8 results. This was probably because of more chondrocytes in these two groups which were involved in the secretion of Col-2 and GAG.

### 3.9. In vitro anti-inflammatory capacity

**3.9.1. Morphology of RAW 264.7.** Macrophages are found in regular spherical shape when they are not activated. After being activated by external stimulation, the number of intracellular mitochondria increases, the cytoplasm becomes larger and the overall shape of the cell is irregular.<sup>53</sup> As shown in Fig. 7A, the inactivated macrophages remained in regular spherical shape after co-culturing with hydrogel specimens. This indicated that macrophages were not activated during co-culturing with hydrogel specimens. Fig. 7B shows the cell shape of LPS-activated macrophages co-cultured with hydrogel specimens. Activated macrophages were observed in all groups, but some macrophages were still observed to remain in an

inactivated state due to the anti-inflammatory ability to inhibit macrophage activation of allicin in hydrogel. Meanwhile, the DCP-contained specimens did not produce additional inflammatory stimuli for RAW264.7 during the co-culture period.

**3.9.2. The secretion of inflammatory factors.** To further evaluate the anti-inflammatory effect of MCOAC hydrogels on RAW264.7 before and after activation, we detected cytokines released from cells in culture supernatants using ELISA kits, and the specific results are shown in Fig. 7C–E. As seen in these data, the secretion of all three pro-inflammatory cytokines from cells in all groups increased significantly after LPS-activation, indicating the successful activation of RAW264.7. The secretion levels of TNF- $\alpha$  and IL-1 $\beta$  from inactivated RAW264.7

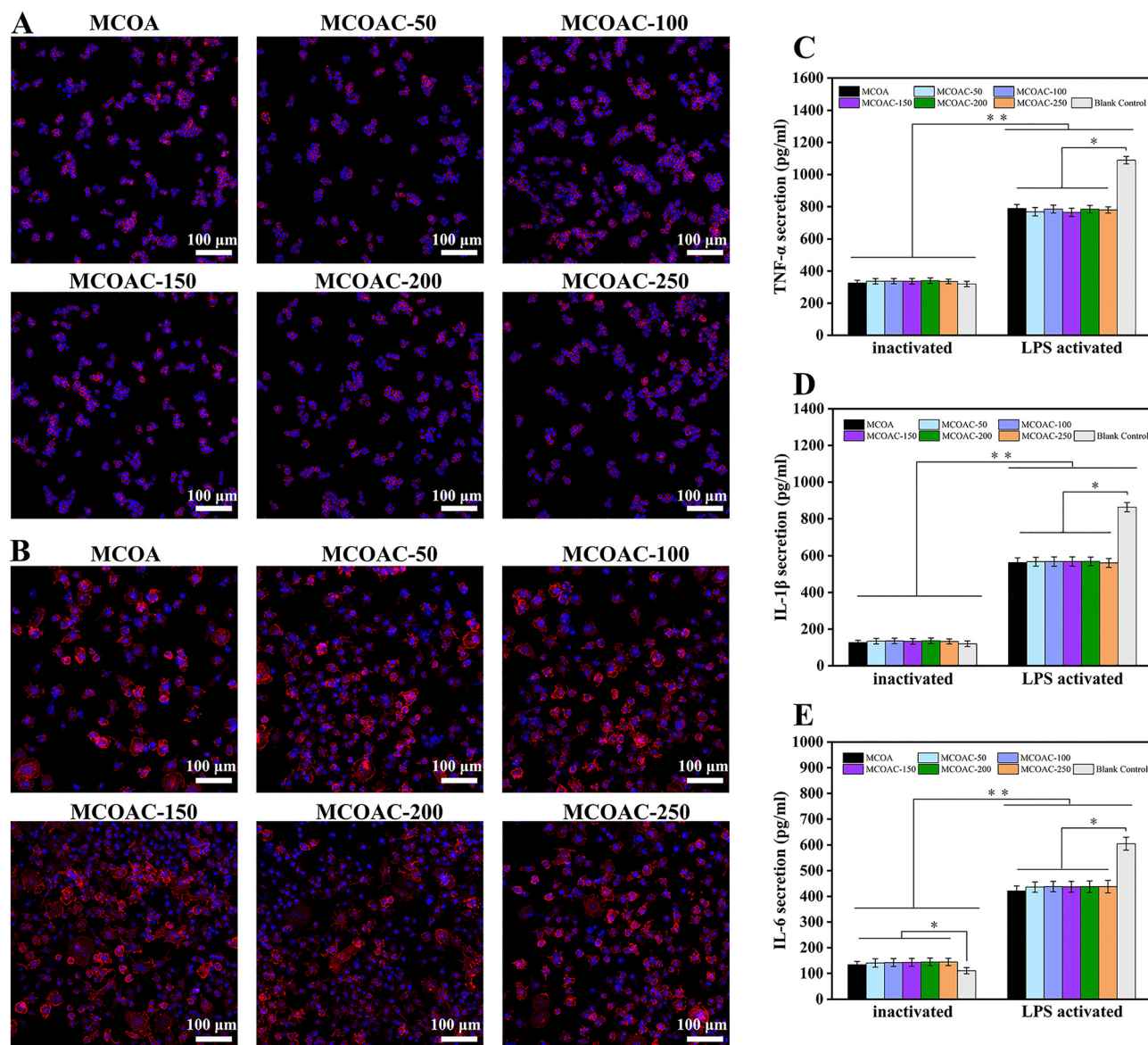
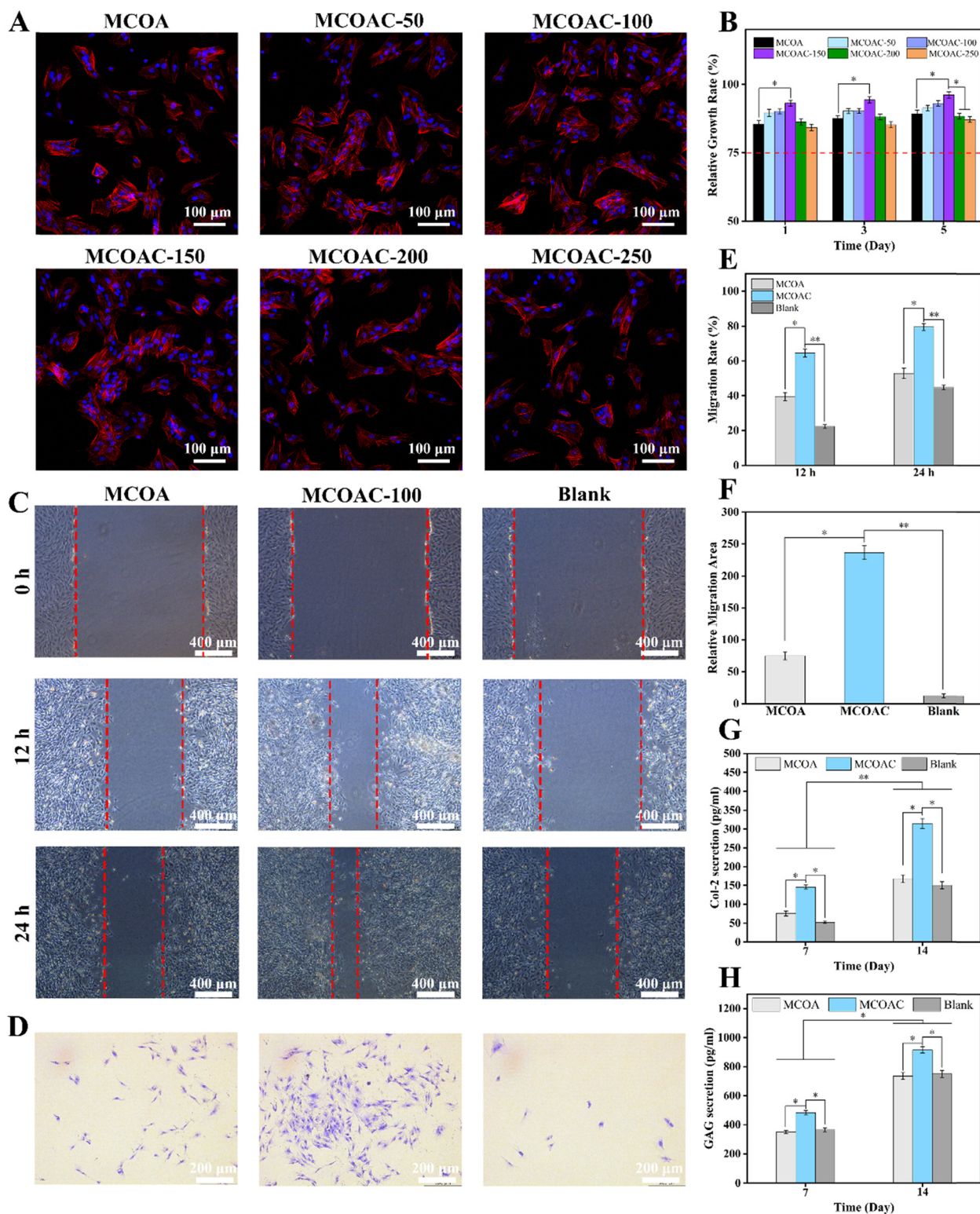


Fig. 7 The RAW264.7 compatibility of hydrogels. (A) CLSM images of inactivated RAW264.7 co-cultured with different hydrogels. (B) CLSM images of activated RAW264.7 co-cultured with different hydrogels. (C) TNF- $\alpha$  secretion from RAW264.7 co-cultured with different hydrogels; (D) IL-1 $\beta$  secretion from RAW264.7 co-cultured with different hydrogels; (E) IL-6 secretion from RAW264.7 co-cultured with different hydrogels. Data are presented as mean  $\pm$  SD ( $n = 6$ ). \* Represents  $p < 0.05$ , \*\* represents  $p < 0.01$ . (one-way ANOVA).

co-cultured with all hydrogels were similar to those of the blank control group, but the expression level of IL-6 was a little higher

than that of the blank control group, indicating that the hydrogels did not activate RAW264.7, while all hydrogels



**Fig. 8** Compatibility of hydrogels with BMSCs. (A) CLSM images of BMSCs co-cultured with different hydrogels. (B) CCK-8 assays of hydrogels. (C) Scratch assay. (D) Transwell assay. (E) Corresponding quantitative data of the scratched area. (F) Corresponding quantitative data of migrating areas. (G) Col-2 secretion from BMSCs. (H) GAG secretion from BMSCs. Data are presented as mean  $\pm$  SD ( $n = 6$ ). \* Represents  $p < 0.05$ , \*\* represents  $p < 0.01$  (one-way ANOVA).

(MCOA and MCOAC) effectively reduced the secretion of three pro-inflammatory cytokines from LPS-activated RAW264.7 co-cultured with samples. This suggested that the introduction of DCP did not decrease the anti-inflammatory ability of hydrogels. The MCOAC hydrogels still had good anti-inflammatory ability.

### 3.10. BMSCs compatibility

**3.10.1. Cytotoxicity assay.** The CCK-8 assay was used to evaluate the effects of MCOAC hydrogels on the proliferation of BMSCs. As shown in Fig. 8B, all hydrogel specimens showed good cytocompatibility with RGR exceeding 75%. The cell viability of the MCOAC hydrogel specimens was better than that of the MCOA hydrogel, indicating that DCP has good ability to promote the proliferation of BMSCs. When the DCP content in hydrogels was high (MCOAC-200 and MCOAC-250), BMSCs co-cultured with hydrogel specimens exhibited a decreasing trend in cell viability similar to that of chondrocytes. This might be due to the excessive degradation of DCP during the co-culture period, leading to the production of some small molecules, which was not conducive to cell growth. However, the low content DCP-contained hydrogels (MCOAC-100 and MCOAC-150) exhibited good ability to promote BMSCs' growth.

**3.10.2. Morphology of BMSCs.** As shown in Fig. 8A, the CLSM image showed that the BMSCs inoculated in all hydrogel specimens spread well, indicating the good BMSC-compatibility of hydrogels. Compared with other hydrogels, more spreading-BMSCs were observed on the surface of the MCOAC-150 hydrogel, which further indicated that a certain concentration of DCP was beneficial to BMSCs' growth.

Based on the previous studies on the physicochemical and antibacterial properties of hydrogel specimens as well as their

cytocompatibility, we selected MCOAC-150 hydrogels for the subsequent experiments.

**3.10.3. Scratch and Transwell assay.** The increased speed of cell migration can promote tissue repair at the site of injury,<sup>54</sup> so we explored the effect of MCOAC-150 hydrogel on BMSC motility. As shown in Fig. 8C (scratch experiment), compared with MCOA hydrogel and blank control groups, the BMSCs co-cultured with MCOAC-150 hydrogel exhibited significant migration at 12 and 24 h, and their migration ratio reached 79.56% at 24 h (Fig. 8E). In Transwell experiment (Fig. 8D), the relative migration area for the MCOAC-150 hydrogel was significantly more than that for the MCOA hydrogel and blank control group (Fig. 8F), indicating that the MCOAC-150 hydrogel could effectively promote the migration of BMSCs. In conclusion, the introduction of DCP was proved to be effective in improving the cell migration of BMSCs through scratch and Transwell experiments, and the MCOAC-150 hydrogel showed the best effect on promoting cell migration, leading to good cartilage tissue repair.

**3.10.4. Cytokine determination.** ELISA analysis unequivocally exposed the production of Col-2 and GAG, which are considered as cartilage matrix-specific proteins. As shown in Fig. 8G and H, during the whole culturing time, the accumulation of Col-2 from BMSCs in all MCOAC hydrogel groups exhibited a marked increase. And the Col-2 content secreted from BMSCs in the MCOAC hydrogel group was significantly higher than that in MCOA and blank control groups at both 7 and 14 days. GAG secretion from BMSCs in MCOAC hydrogel groups showed a similar variation trend in accordance with Col-2. In conclusion, the DCP-contained MCOAC hydrogels could promote the differentiation of BMSCs to chondrocytes, which is beneficial for repairing cartilage defective tissues.

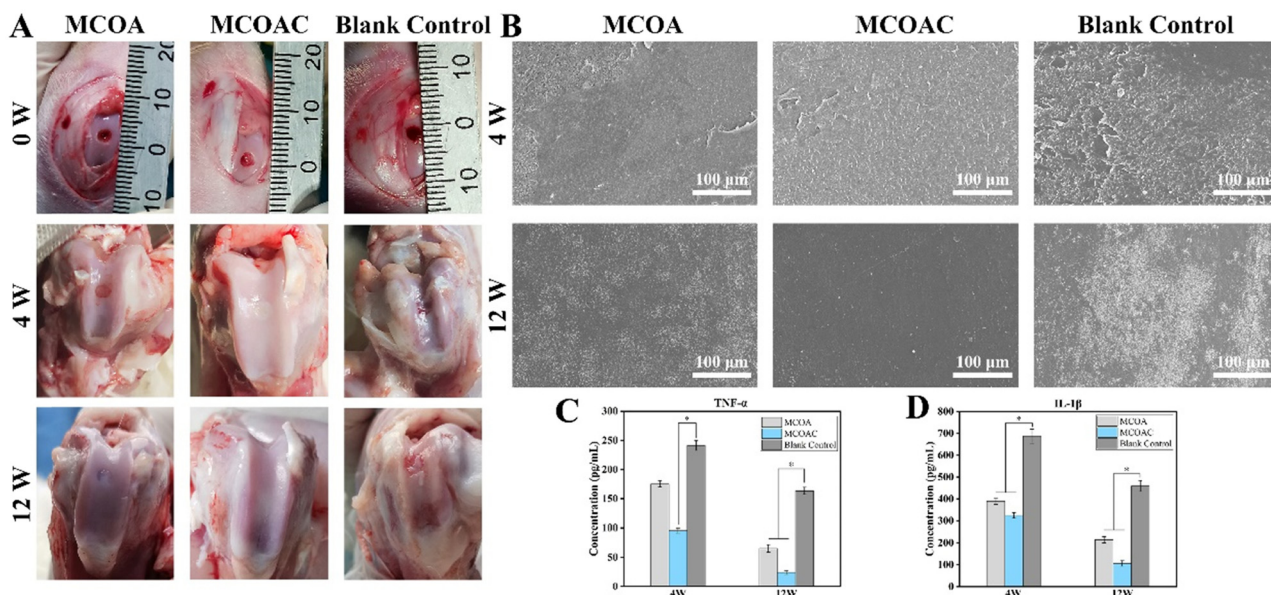


Fig. 9 Patellar wear and inflammation in the joint cavity. (A) Actual healing of the cartilage defect. (B) SEM images of patellar wear. (C) TNF- $\alpha$  content in the joint cavity. (D) IL-1 $\beta$  content in the joint cavity. Data are presented as mean  $\pm$  SD ( $n = 6$ ). \* Represents  $p < 0.05$  (one-way ANOVA).

### 3.11. *In vivo* cartilage repair

**3.11.1. Actual healing and patellar wear.** Knee motion after cartilage damage would rub and damage the patellar surface and produce joint inflammation. We investigated the anti-inflammatory and pro-chondral repair effects of MCOAC hydrogel *in vivo* by measuring patellar wear and inflammation in the joint cavity. Fig. 9A shows that the actual cartilage healing in the MCOAC group was better than that in the blank control and MCOA groups at 4 postoperative weeks. At 12 weeks, the inflammatory condition around the defect site was reduced in all groups, but the cartilage defect wound in the blank control group did not heal completely, while the MCOAC group presented a better wound healing capacity than the MCOA group, indicating the good ability of the MCOAC hydrogel to promote cartilage repair.

The surface morphology of patella at two time points is shown in Fig. 9B. At 4 postoperative weeks, all groups exhibited

some degree of patellar surface wear due to early inflammation, but the blank control group showed more severe patellar surface wear than that of MCOA and MCOAC groups. This was because the filling of hydrogel effectively reduced the friction between the patella and the cartilage defect. At 12 weeks, there was no significant wear on the patellar surface in the MCOAC group, which was due to the gradual disappearance of inflammation and gradual repair of cartilage with the elapse of time. However, the patellar surface of the blank control group still showed severe wear because the cartilage in the blank control group was poorly healed and underwent rubbing against the patella. And the degree of patellar surface wear in the MCOA group was between the MCOAC group and the blank control group.  $\text{TNF-}\alpha$  and  $\text{IL-1}\beta$  are the most dominant proinflammatory cytokines in OA pathology.  $\text{TNF-}\alpha$  not only increases the death of chondrocyte and cartilage matrix breakdown but also inhibits the production of GAGs and Col-2 from chondrocyte.  $\text{IL-1}\beta$  inhibits the synthesis of Col-2 and GAGs and upregulates

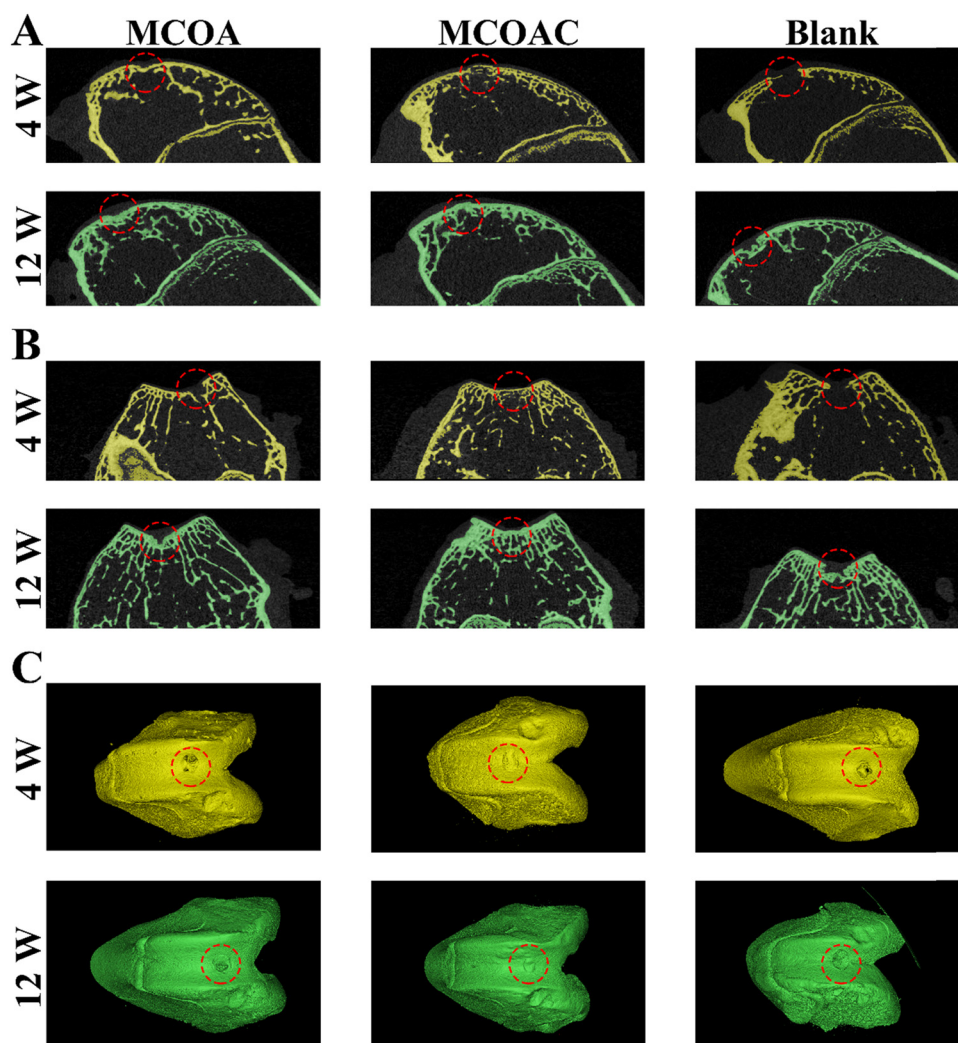


**Fig. 10** Micro-CT images for two time points. (A) 2D reconstruction in the landscape view (red squares indicated the defect areas). (B) 2D reconstruction in the longitudinal view (red squares indicated the defect areas). (C) 3D reconstruction (red circles indicated the defect areas). Yellow represents the reconstruction results of 4 weeks and green represents the reconstruction results of 12 weeks.

the production of metallo-matrix protease, which promoted the degradation of ECM. The content of  $\text{TNF-}\alpha$  and  $\text{IL-1}\beta$  in the joint fluid is shown in Fig. 9C and D. At 4 weeks, all groups exhibited high  $\text{TNF-}\alpha$  and  $\text{IL-1}\beta$  expression, which indicated that all groups had some degree of inflammation in the early stages of cartilage repair. However, the expression of both cytokines in the blank control group was significantly higher than that in the MCOAC hydrogel group, suggesting that the MCOAC hydrogel had some degree of anti-inflammatory ability in the early stage of cartilage repair. The expression of both inflammatory factors showed a decreasing trend at 12 postoperative weeks compared with that at 4 postoperative weeks, which was similar to the actual healing situation. Meanwhile, the expression of inflammatory factors in the blank control group was still significantly higher than that in MCOA and MCOAC groups, which indicated that in the late stage of cartilage repair, the hydrogel could effectively reduce inflammation at the cartilage defect and provide a good microenvironment for cartilage repair. In conclusion, MCOAC hydrogel can effectively promote cartilage repair at the defect, lower the patellar surface wear and reduce inflammation in the knee joint, and is considered an excellent hydrogel for cartilage repair.

**3.11.2. Micro-CT reconstruction evaluation.** In animal experiment, a full-thickness cartilage defect was used as the defect model, which stretched deep beneath the tidemark, without penetrating the subchondral bone plate. As shown in the lateral (Fig. 10A and B) and 3D (Fig. 10C) reconstruction

images, the newly regenerated tissue generally grew from the margin of defects to the central areas. After 4 postoperative weeks, the defect treated with MCOAC hydrogel was partially covered with new cartilage, and the restoration of the defect site in the MCOAC group was better than that in the blank control group and MCOA group. After 12 postoperative weeks, the defect in the MCOAC group was almost repaired, and a regenerated matching cartilage layer was formed. In contrast, the restoration of the defects in the other two groups was poor, and there still existed a blank zone at the site of defects after 12 weeks.

**3.11.3. Histological analysis.** Articular cartilage repair was further explored and analyzed by histological staining. It can be seen in Fig. 11 that among all experimental groups, better cartilage repair was observed at both 4 and 12 weeks. At 4 weeks, the MCOAC hydrogel group was able to observe significant neointimal tissue at the defect site, but the fibrous arrangement of neointimal tissue showed a disorganized nature. In contrast, the blank control group showed a poor degree of cartilage repair, in which the new tissue did not yet fully grow over the wound. The MCOA group showed better cartilage repair than the blank control group but less fibrous deposition at the defect site than that of the MCOAC group. At 12 weeks, the cartilage repair was good in MCOAC and MCOA groups with intact perichondrium and the cartilage layer thickness was the same as that of the normal site cartilage tissue, but the chondrocytes in the MCOA group were scattered and did not form an isogenous group. In the blank control group, the

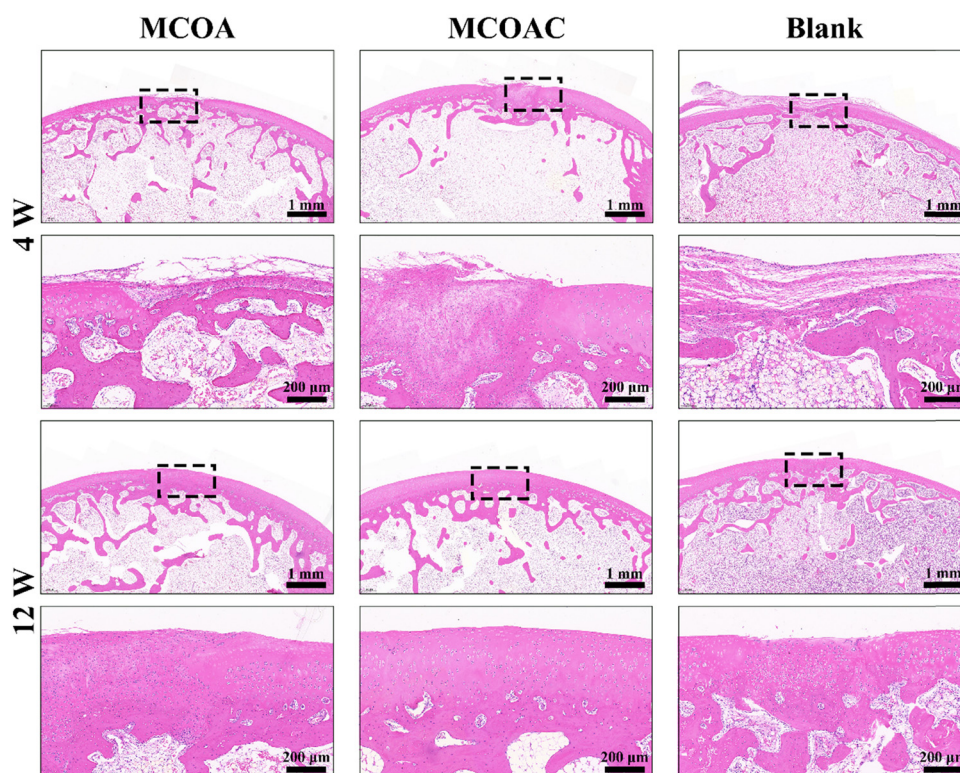


Fig. 11 H&E immunohistochemical staining for cartilage defect repair *in vivo*.

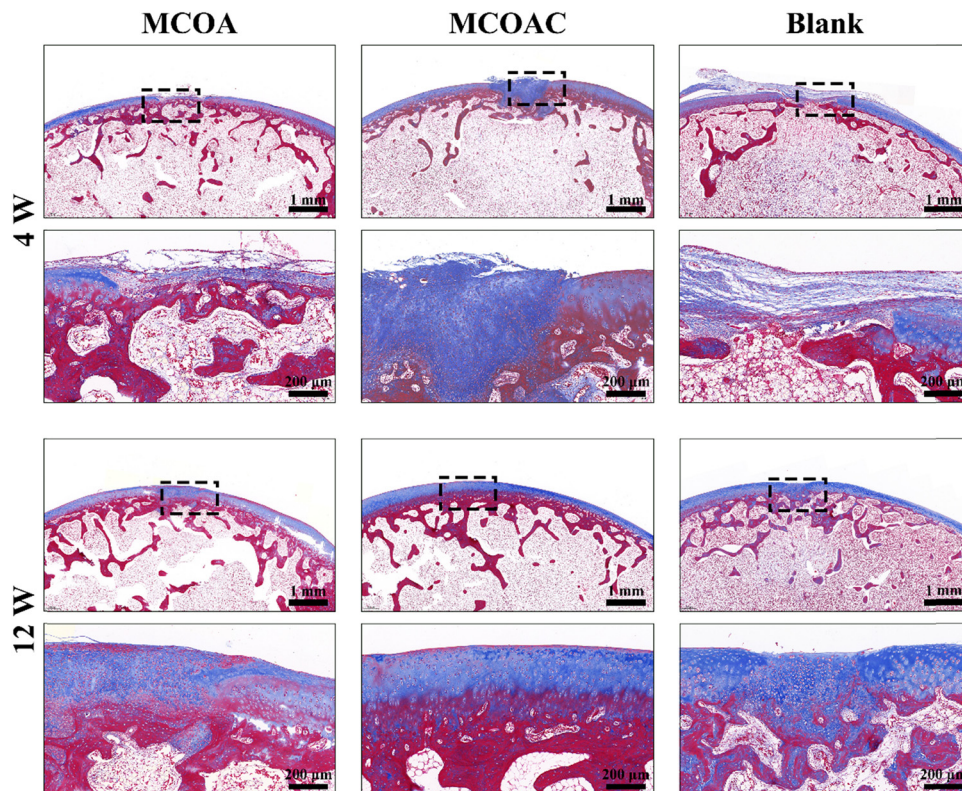


Fig. 12 Masson immunohistochemical staining for cartilage defect repair *in vivo*.

perichondrium was not completely healed, the collagen fibers could be observed in new tissue and the fibrocartilage was formed. The cartilage capsule was observed in the MCOAC group, and the cartilage matrix was significantly different from that of the blank control group, forming hyaline cartilage.

The Masson staining results are shown in Fig. 12. At 4 weeks, the number of new collagen fibers in the MCOAC group was much higher than that in the blank control and MCOA groups, which further indicated that the MCOAC group was able to promote chondrocytes to secrete more collagen and promote cartilage repair in the early stage of cartilage repair. At 12 weeks, the collagen in the MCOAC group gradually matured and showed a clear hyaline cartilage matrix. In contrast, the collagen fibers of the blank control group remained disordered, and the new cartilage tissue was fibrocartilage. In conclusion, the DCP-contained MCOAC hydrogels could effectively promote cartilage repair at joint defects. The MCOAC hydrogel is a promising hydrogel for cartilage repair by promoting relevant cells to secrete more collagen and eventually form hyaline cartilage.

## 4. Conclusion

In summary, we prepared a stable hydrogel using MA-CMCS and OLBG, and endowed the hydrogels with good antibacterial and anti-inflammatory properties as well as enhanced cartilage repair abilities by loading allicin and DCP into hydrogels. FTIR and  $^1\text{H}$  NMR spectra indicated the successful preparation of

MA-CMCS and OLBG. H&E staining, SEM images and changes in DNA and Col-2 contents before and after decellularization demonstrated the success of cartilage decellularization. The SEM images demonstrated that the hydrogels had formed a three-dimensional network structure, and the rheological properties showed that various hydrogels had good stability. The introduction of allicin could improve the antibacterial ability of MCOAC hydrogel specimens, which was confirmed through the antibacterial experiments of *S. aureus* and *E. coli*. Meanwhile, the MCOAC hydrogel was also able to effectively inhibit the secretion of pro-inflammatory cytokines from LPS-activated RAW264.7 co-cultured with hydrogel specimens. The introduction of DCP improved the chondrocyte compatibility of hydrogels, and the ability of the DCP-contained MCOAC hydrogel to promote the differentiation of BMSCs to chondrocytes was demonstrated through scratch and Transwell assay as well as the expression of relevant chondrocyte signature factors. More importantly, DCP-contained hydrogel specimens were shown to be effective in promoting cartilage tissue growth and wound healing in articular cartilage defects *in vivo*. Overall, the DCP-contained MCOAC hydrogel is an excellent and promising hydrogel for cartilage repair.

## Author contributions

Can Cheng: conceptualization, methodology, data curation, and writing – original draft. Xu Peng: investigation and visualization. Yihao Luo: investigation and data curation. Shubin

Shi: methodology and software. Ling Wang: investigation and formal analysis. Yuhang Wang: investigation and formal analysis. Xixun Yu: funding acquisition, writing – review & editing and supervision.

## Ethical approval

All institutional and national guidelines for the care and use of laboratory animals were followed.

## Conflicts of interest

The authors declare that they have no conflict of interest.

## Acknowledgements

This work was supported by the National Key Research and Development Program of China (No. 2016YFC1100900, No. 2016YFC1100901, No. 2016YFC1100903, and No. 2016YFC1100904), and “From 0 to 1” innovative research projects of Sichuan University (2022SCUH0045).

## References

- 1 Z. Peng, H. Sun, V. Bunpetch, Y. Koh, Y. Wen, D. Wu and H. Ouyang, *Biomaterials*, 2021, **268**, 120555.
- 2 X. Nie, Y. J. Chuah, W. Zhu, P. He, Y. Peck and D. A. Wang, *Biomaterials*, 2020, **235**, 119821.
- 3 J. Zhang, B. Li, J. Zuo, R. Gu, B. Liu, C. Ma, J. Li and K. Liu, *Adv. Healthcare Mater.*, 2021, **10**, e2100109.
- 4 H. Martinez Avila, E. M. Feldmann, M. M. Pleumeekers, L. Nimeskern, W. Kuo, W. C. de Jong, S. Schwarz, R. Muller, J. Hendriks, N. Rotter, G. J. van Osch, K. S. Stok and P. Gatenholm, *Biomaterials*, 2015, **44**, 122–133.
- 5 A. R. Armiento, M. J. Stoddart, M. Alini and D. Eglin, *Acta Biomater.*, 2018, **65**, 1–20.
- 6 W. Wei, Y. Ma, X. Yao, W. Zhou, X. Wang, C. Li, J. Lin, Q. He, S. Leptihn and H. Ouyang, *Bioact Mater*, 2021, **6**, 998–1011.
- 7 H. Park, H. J. Lee, H. An and K. Y. Lee, *Carbohydr. Polym.*, 2017, **162**, 100–107.
- 8 D. Y. Kim, H. Park, S. W. Kim, J. W. Lee and K. Y. Lee, *Carbohydr. Polym.*, 2017, **157**, 1281–1287.
- 9 Z. Ye, H. Lu, E. Jia, J. Chen and L. Fu, *Polym. Adv. Technol.*, 2022, **33**, 3455–3469.
- 10 Z. Yin, D. Li, Y. Liu, S. Feng, L. Yao, X. Liang, C. Miao, Y. Xu, M. Hou, R. Zhang, W. Zhang, W. Liu, Y. Liu, G. Zhou and Y. Cao, *Appl. Mater. Today*, 2020, **20**, 100724.
- 11 Y. P. Singh, N. Bhardwaj and B. B. Mandal, *ACS Appl. Mater. Interfaces*, 2016, **8**, 21236–21249.
- 12 Y. Xu, L. Jia, Z. Wang, G. Jiang, G. Zhou, W. Chen and R. Chen, *Mater. Lett.*, 2020, **268**, 127609.
- 13 J. Wu, Q. Ding, A. Dutta, Y. Wang, Y. H. Huang, H. Weng, L. Tang and Y. Hong, *Acta Biomater.*, 2015, **16**, 49–59.
- 14 C. Yang, L. Gong, X. Li, W. Li, X. Meng and B. Liu, *Food Chem.*, 2023, **404**, 134526.
- 15 M. Suneetha, S. Y. Won, S. M. Zo and S. S. Han, *Gels*, 2023, **9**, 184.
- 16 X. Wu, Q. Zhang, Z. Wang, Y. Xu, Q. Tao, J. Wang, X. Kong, K. Sheng and Y. Wang, *Int. J. Biol. Macromol.*, 2022, **209**, 1837–1847.
- 17 J. Chen, L. Luo, C. Cen, Y. Liu, H. Li and Y. Wang, *Int. J. Biol. Macromol.*, 2022, **220**, 462–471.
- 18 Y. Min, R. Han, G. Li, X. Wang, S. Chen, M. Xie and Z. Zhao, *Adv. Funct. Mater.*, 2023, **33**, 2212803.
- 19 L. Wang, X. Gang, Y. Xiao, Y. Ren, J. Wang, B. Niu and W. Li, *Eur. Polym. J.*, 2023, **192**, 112069.
- 20 Z. Liu, X. Mo, F. Ma, S. Li, G. Wu, B. Tang and L. Lin, *Carbohydr. Polym.*, 2021, **261**, 117869.
- 21 Y. Qu, S. He, S. Luo, J. Zhao, R. Liang, C. Liao and L. Zheng, *Adv. Healthcare Mater.*, 2023, e2203079, DOI: [10.1002/adhm.202203079](https://doi.org/10.1002/adhm.202203079).
- 22 B. Basyigit, G. Altun, M. Yucetepe, A. Karaaslan and M. Karaaslan, *Int. J. Biol. Macromol.*, 2023, **231**, 123352.
- 23 F. Mendes de Moraes, S. C. Trauthman, F. Zimmer, P. P. Pacheco, F. D. Pont Morisso, A. L. Ziulkoski, L. A. Kanis and Z. Karine Modolon, *Sustainable Chem. Pharm.*, 2022, **25**, 100604.
- 24 M. Petitjean, N. Lamberto, A. Zornoza and J. R. Isasi, *Carbohydr. Polym.*, 2022, **288**, 119387.
- 25 D. Yun, Y. He, H. Zhu, Y. Hui, C. Li, D. Chen and J. Liu, *Int. J. Biol. Macromol.*, 2022, **205**, 141–153.
- 26 R. Wang, S. Zhang, S. Liu, Y. Sun and H. Xu, *Polymers*, 2023, **15**, 1751.
- 27 G. H. Matar, M. Andac and A. Elmas, *J. Appl. Polym. Sci.*, 2021, **139**, 51498.
- 28 S. Kaity, J. Isaac, P. M. Kumar, A. Bose, T. W. Wong and A. Ghosh, *Carbohydr. Polym.*, 2013, **98**, 1083–1094.
- 29 C. R. Rowland, L. A. Colucci and F. Guilak, *Biomaterials*, 2016, **91**, 57–72.
- 30 M. Gong, J. Sun, G. Liu, L. Li, S. Wu and Z. Xiang, *Mater. Sci. Eng., C*, 2021, **119**, 111603.
- 31 H. V. Almeida, Y. Liu, G. M. Cuniffe, K. J. Mulhall, A. Matsiko, C. T. Buckley, F. J. O'Brien and D. J. Kelly, *Acta Biomater.*, 2014, **10**, 4400–4409.
- 32 L. Luo, R. Eswaramoorthy, K. J. Mulhall and D. J. Kelly, *J. Mech. Behav. Biomed. Mater.*, 2015, **55**, 21–31.
- 33 A. F. Elsaesser, C. Bermueller, S. Schwarz, L. Koerber, R. Breiter and N. Rotter, *Tissue Eng., Part A*, 2014, **20**, 1668–1678.
- 34 J. Visser, D. Gawlitta, K. E. Benders, S. M. Toma, B. Pouran, P. R. van Weeren, W. J. Dhert and J. Malda, *Biomaterials*, 2015, **37**, 174–182.
- 35 C. H. Chang, C. C. Chen, C. H. Liao, F. H. Lin, Y. M. Hsu and H. W. Fang, *J. Biomed. Mater. Res., Part A*, 2014, **102**, 2248–2257.
- 36 J. Reiter, A. M. Hubbers, F. Albrecht, L. I. O. Leichert and A. J. Slusarenko, *Int. J. Med. Microbiol.*, 2020, **310**, 151359.
- 37 S. Bose, A. Bhattacharjee, C. Huynh and D. Banerjee, *JOM*, 2022, **74**, 3349–3356.
- 38 Q. Zha, X. Wang, X. Cheng, S. Fu, G. Yang, W. Yao and R. Tang, *Mater. Sci. Eng., C*, 2017, **78**, 246–257.
- 39 X. Xing, J. Su, Y. Liu, H. Lin, Y. Wang and H. Cheng, *Colloids Surf., B*, 2022, **218**, 112760.

- 40 C. Cheng, X. Peng, L. Xi, Y. Luo, Y. Wang, Y. Zhou and X. Yu, *J. Biomed. Mater. Res., Part A*, 2023, **111**, 170–184.
- 41 H. V. Almeida, R. Eswaramoorthy, G. M. Cunniffe, C. T. Buckley, F. J. O'Brien and D. J. Kelly, *Acta Biomater.*, 2016, **36**, 55–62.
- 42 C. Cheng, X. Peng, L. Xi, C. Wan, S. Shi, Y. Wang and X. Yu, *Food Funct.*, 2022, **13**, 9622.
- 43 C. Wan, M. Hu, X. Peng, N. Lei, H. Ding, Y. Luo and X. Yu, *Biomater. Sci.*, 2022, **10**, 6291–6306.
- 44 Y. F. Poon, Y. B. Zhu, J. Y. Shen, M. B. Chan-Park and S. C. Ng, *Adv. Funct. Mater.*, 2007, **17**, 2139–2150.
- 45 W. Kang, B. Bi, R. Zhuo and X. Jiang, *Carbohydr. Polym.*, 2017, **160**, 18–25.
- 46 Y. Zhao, Y. Li, X. Peng, X. Yu, C. Cheng and X. Yu, *Int. J. Biol. Macromol.*, 2021, **184**, 831–842.
- 47 V. P. Ribeiro, A. da Silva Morais, F. R. Maia, R. F. Canadas, J. B. Costa, A. L. Oliveira, J. M. Oliveira and R. L. Reis, *Acta Biomater.*, 2018, **72**, 167–181.
- 48 S. Bhattacharya, D. Sen and C. Bhattacharjee, *Process Biochem.*, 2022, **122**, 110–119.
- 49 Z. Chang, L. An, Z. He, Y. Zhang, S. Li, M. Lei, P. Xu, Y. Lai, Z. Jiang, Y. Huang, X. Duan and W. Wu, *Food Funct.*, 2022, **13**, 3495–3511.
- 50 H. Yuan, L. L. E. Mears, X. Liu, W. Qi, R. Su and M. Valtiner, *Colloids Surf., B*, 2022, **220**, 112906.
- 51 L. Veenendaal, A. Longoni, G. J. Hooper, K. S. Lim, T. B. F. Woodfield and G. C. J. Lindberg, *Adv. Mater. Interfaces*, 2022, **9**, 2200882.
- 52 J. Marchan, O. Wittig, D. Diaz-Solano, M. Gomez and J. E. Cardier, *Injury*, 2022, **53**, 399–407.
- 53 Y. Sun, T. Liu, H. Hu, Z. Xiong, K. Zhang, X. He, W. Liu, P. Lei and Y. Hu, *Mater. Today Bio*, 2022, **16**, 100340.
- 54 C. Lin, B. Tao, Y. Deng, Y. He, X. Shen, R. Wang, L. Lu, Z. Peng, Z. Xia and K. Cai, *Biomaterials*, 2019, **217**, 119300.